Substrate Specificity and Kinetic Mechanism of the Sir2 Family of NAD$^+$-Dependent Histone/Protein Deacetylases†

Margie T. Borra,‡ Michael R. Langer,§ James T. Slama,|| and John M. Denu*,‡

Department of Biomolecular Chemistry, University of Wisconsin, Madison, Wisconsin 53706-1532, Department of Biochemistry and Molecular Biology, Oregon Health and Science University, Portland, Oregon 97329-3098, and Department of Medicinal and Biological Chemistry, University of Toledo College of Pharmacy, Toledo, Ohio 43606-3390

Received February 27, 2004; Revised Manuscript Received May 24, 2004

ABSTRACT: The Silent information regulator 2 (Sir2) family of enzymes consists of NAD$^+$-dependent histone/protein deacetylases that tightly couple the hydrolysis of NAD$^+$ and the deacetylation of an acetylated substrate to form nicotinamide, the deacetylated product, and the novel metabolite *O*-acetyl-ADP-ribose (*O*AADPR). In this paper, we analyzed the substrate specificity of the yeast Sir2 (ySir2), the yeast HST2, and the human SIRT2 homologues toward various monoacetylated histone H3 and H4 peptides, determined the basic kinetic mechanism, and resolved individual chemical steps of the Sir2 reaction. Using steady-state kinetic analysis, we have shown that ySir2, HST2, and SIRT2 exhibit varying catalytic efficiencies and display a preference among the monoacetylated peptide substrates. Bisubstrate kinetic analysis indicates that Sir2 enzymes follow a sequential mechanism, where both the acetylated substrate and NAD$^+$ must bind to form a ternary complex, prior to any catalytic step. Using rapid-kinetic analysis, we have shown that after ternary complex formation, nicotinamide cleavage occurs first, followed by the transfer of the acetyl group from the donor substrate to the ADP-ribose portion of NAD$^+$ to form *O*AADPr and the deacetylated product. Product and dead-end inhibition analyses revealed that nicotinamide is the first product released followed by random release of *O*AADPr and the deacetylated product.

Reversible acetylation is emerging as a major regulatory mechanism for histone and non-histone proteins involved in transcription, apoptosis, and other cellular functions (*1*, *2*). It is becoming clearer that several histone acetyltransferases (HATs)[1] and histone deacetylases (HDACs) utilize non-histone proteins as physiological substrates, leading to some reservations about referring to these enzymes as "histone"-modifying enzymes. Nonetheless, there are three classes of so-called histone deacetylases (*2*, *3*), which are classified on the basis of their similarity to yeast enzymes. Unique among the deacetylases are class III deacetylases, which make up the Silent information regulator 2 (Sir2) family (*3*, *4*). Unlike the class I and II enzymes, class III deacetylases are absolutely dependent on NAD$^+$ for activity (*3*, *4*). The founding member of the Sir2 enzymes, also termed sirtuins (*5*), is the yeast Sir2 (ySir2), which has been shown to be essential for gene silencing at the three yeast silent loci (*3*, *4*).

Sir2 proteins possess robust NAD$^+$-dependent deacetylase activity (*6*−*8*) that tightly couples the cleavage of NAD$^+$ and protein deacetylation to produce nicotinamide, the deacetylated product, and a unique compound *O*-acetyl-ADP-ribose (*O*AADPR) (*9*−*13*). It has been estimated that the deacetylase activity of a yeast homologue HST2 is 1000-fold higher than its ADP-ribosyl transferase activity (*9*). In a few cases, physiological protein targets for some Sir2-like proteins have been suggested, though most remain largely unknown. Human SIRT1 (or its mouse homologue, Sir2α) was shown to deacetylate tumor suppressor p53 (*14*−*16*) and transcription factor TAF$_I$68 (*17*). Acetyl-CoA synthetase is a target of the bacterial Sir2 (*18*), and α-tubulin can be deacetylated by human SIRT2 (*19*). The yeast Sir2 is localized to loci where chromatin (namely, H3 and H4) are hypoacetylated (*20*, *21*), making a strong case that ySir2 is a bona fide histone deacetylase and that its enzymatic activity induces silent chromatin. Nearly all Sir2 enzymes have been shown to catalyze the deacetylation of histone proteins or peptides, although no study has investigated the substrate preference and catalytic efficiency of Sir2 enzymes for histone substrates in a quantitative manner.

Recently determined crystal structures of Sir2-Af2 from *Archaeoglobus fulgidus*, bound to an acetylated p53 peptide, and yeast HST2 in a ternary complex with a histone H4

† This work was supported by American Cancer Society Grant RSG-01-029-01 and NIH Grant RO1 GM65386 to J.M.D. and NIH Predoctoral Fellowship F31 GM066366 to M.T.B.

* To whom correspondence should be addressed: Department of Biomolecular Chemistry, University of Wisconsin, 1300 University Ave., Madison, WI 53706. Phone: (608) 265-1859. Fax: (608) 262-5253. E-mail: jmdenu@wisc.edu.

‡ University of Wisconsin.

§ Oregon Health and Science University.

|| University of Toledo College of Pharmacy.

[1] Abbreviations: Sir2, silent information regulator 2; HST2, homologue of Sir2 (in yeast); SIRT2, human homologue of Sir2; *O*AADPr, *O*-acetyl-ADP-ribose; HATs, histone acetyltransferases; HDACs, histone deacetylases; NAD$^+$, nicotinamide adenine dinucleotide; IPTG, isopropyl β-D-thiogalactopyranoside; HPLC, high-performance liquid chromatography; TFA, trifluoroacetic acid; ITC, isothermal titration calorimetry; AcH4, acetylated histone H4 peptide (the number in parentheses indicates the location of the acetyl group); AcH3, acetylated histone H3 peptide (the number in parentheses indicates the location of the acetyl group); H3, unmodified histone H3 peptide.

10.1021/bi049592e CCC: $27.50
Published on Web 07/10/2004

peptide and 2′-*O*AADPr suggested that Sir2 enzymes exhibit little specificity (*22*, *23*). In both cases, the peptide substrate binds to a cleft between the two domains, forming an enzyme−substrate β-sheet, and the acetyllysine side chain is buried in a conserved hydrophobic pocket, which positions the acetyl group in the proximity of the predicted nicotinamide ribose binding site (*22*, *23*). The predominance of backbone interactions between the peptide substrate and enzyme led the authors of the two studies to conclude that residues flanking the acetyllysine group contribute minimally to substrate recognition and specificity (*22*, *23*). Overall, Sir2 enzymes are composed of a large subdomain containing a Rossmann fold and a smaller zinc-binding subdomain (*13*, *22*−*26*). The NAD^+ binding site is located in the cleft between the two domains. Crystallographic evidence showing 2′-*O*AADPR in the active site (*13*, *23*) is consistent with the previously published biochemical evidence which shows that 2′-*O*AADPR is the enzymatic product of the reaction (*11*, *12*).

How Sir2 enzymes catalyze substrate deacetylation and form *O*AADPr is not clearly understood. Several mechanisms have been proposed (*23*, *27*, *28*); however, no detailed kinetic analyses have been performed. The proposed mechanisms suggest an enzyme-ADP-ribose-like intermediate is formed, an aspect of the reaction that was also established by the observation of a nicotinamide−NAD^+ exchange reaction (*8*, *27*−*29*). However, a complete steady-state kinetic mechanism for a Sir2 enzyme has not been described. Moreover, supportive evidence for distinct chemical steps in the reaction is lacking.

This paper focuses on three main goals: determining the inherent differences in catalytic efficiency and substrate preference among Sir2 enzymes for various histone peptides, establishing the overall kinetic mechanism, and resolving individual chemical steps of the Sir2 reaction. We determined the steady-state kinetic parameters K_m, k_{cat}, and k_{cat}/K_m with three different Sir2 family members (ySir2, yeast HST2, and human SIRT2) using various monoacetylated histone H3 and H4 peptides. Our results show that ySir2, HST2, and SIRT2 can discriminate among the different peptide substrates, as well as display differences in catalytic efficiency. Also, Sir2-like enzymes follow a sequential mechanism, in which NAD^+ and acetylated substrate must bind to form a ternary complex prior to catalysis. Nicotinamide is the first product to be released, followed by a random release of the deacetylated product and *O*AADPR. After the ternary complex has been established, product formation occurs in two distinct chemical steps, with nicotinamide cleavage preceding the transfer of the acetyl group from the donor substrate to the ADP-ribose portion of NAD^+ to form *O*AADPr and the deacetylated product.

EXPERIMENTAL PROCEDURES

Materials. The plasmid containing the full-length, histidine-tagged HST2, pJWLO3, was obtained from R. Sternglanz from the State University of New York (Stony Brook, NY). The plasmid containing the human sirtuin, SIRT2, was obtained from E. Verdin from the University of California (San Francisco, CA). The plasmid containing the yeast Sir2 was obtained from R.-M. Xu from Cold Spring Harbor Laboratory (Cold Spring Harbor, NY). Monoacetylated and unacetylated H3 and H4 peptides, corresponding to the 20 N-terminal residues of histones H3 and H4, respectively, were purchased from the Protein Chemistry Core Lab at the Baylor College of Medicine (Houston, TX). The 11-residue H3 peptide, which corresponds to the 11 residues surrounding and including lysine 14 of histone H3, was purchased from SynPep Corp. (Dublin, CA). AcH3(K9) was a generous gift from C. D. Allis from the University of Virginia Health Sciences Center (Charlottesville, VA). [^{3}H]Acetylcoenzyme A and [^{14}C]nicotinamide were purchased from NEN Life Sciences Products. All other reagents were of the highest commercially available quality.

Expression and Purification. Expression and purification of HST2 and SIRT2 were previously described (*30*). The plasmid containing ySir2 was transformed into XL1-Blue cells, and cells were grown on 2× YT medium with 100 mg/L ampicillin. Cells were grown to an OD_{600} of 0.6−0.8 prior to induction with isopropyl β-D-thiogalactopyranoside (IPTG) for 3−8 h.

The ySir2 was purified using the same protocol as described for HST2 except that 1 M NaCl was added to all purification buffers. The final dialysis buffer contained 300 mM NaCl. All proteins were concentrated and stored at −20 °C until they were used.

Sir2 Deacetylation Assays. The HPLC-based deacetylation assay was employed to determine the substrate specificity of the various Sir2 homologues. HPLC-based assays were performed as previously described (*30*, *31*).

A charcoal binding assay was developed (*27*, *31*) and was used to determine the kinetic mechanism of the Sir2 reaction. The charcoal binding assay is performed using [^{3}H]AcH3 [making of this substrate was previously described (*30*)] and takes advantage of the differential binding of substrates and products to activated charcoal. At high pH (≥9.5) and high temperature, the acetyl group from the [^{3}H]*O*AADPr product is hydrolyzed and can be separated from the rest of the charcoal-bound substrates and products. Because the charcoal binding assay is less time-consuming and allows detection of products at low [^{3}H]AcH3 concentrations, this assay was used to perform the bisubstrate and the product inhibition analyses as well as to determine the substrate preference of ySir2, HST2, and SIRT2 for the AcH3 peptide.

Determination of the Substrate Preference. The HPLC-based assay was used to determine the catalytic efficiency and substrate preference of HST2, SIRT2, and ySir2 for various monoacetylated H3 and H4 peptides. The reactions were performed in the presence of increasing concentrations of peptide, a saturating concentration of NAD^+, and a catalytic amount of the enzyme. Time points were chosen such that steady-state initial velocities were maintained in all reactions. Amounts of products were quantified as described in the assay. Graphs of rate (inverse seconds) versus the concentration of acetylated peptide were fitted to the Michaelis−Menten equation (eq 1), using Kaleidagraph, to obtain the kinetic parameters K_m, k_{cat}, and k_{cat}/K_m.

$$v_o = (k_{cat}[S])/(K_m + [S]) \quad (1)$$

Bisubstrate Kinetic Measurements. Bisubstrate kinetic analyses were performed with SIRT2 at 37 °C in 1 mM DTT and 50 mM Tris (pH 7.5) using the charcoal binding deacetylation assay as previously described (*27*, *31*). The

assay was performed in the presence of NAD^+ concentrations from 25 to 400 μM, [^{3}H]AcH3 concentrations from 15 to 200 μM, and 100 nM SIRT2. The [^{3}H]AcH3 (monoacetylated at Lys-14) was made using P/CAF as previously described (*30*). The initial velocity data were fitted to two possible kinetic mechanisms, sequential (eq 2) and ping-pong (eq 3), using the algorithms of Cleland (*32*) and the computer program KinetAssyst (IntelliKinetics, State College, PA), using a nonlinear least-squares approach.

$$v = (V_m[A][B])/(K_aK_b + K_{ma}[B] + K_{mb}[A] + [A][B]) \quad (2)$$

$$v = (V_m[A][B])/(K_{ia}K_b + K_{ma}[B] + K_{mb}[A] + [A][B]) \quad (3)$$

Product and Dead-End Inhibition Analyses. Product inhibition analyses were performed using SIRT2 at 37 or 25 °C in 50 mM Tris (pH 7.5 at 37 °C) and 1 mM DTT. For all inhibition analyses, the AcH3 refers to the 11-mer [^{3}H]-AcH3, monoacetylated at Lys-14 using P/CAF as described in Experimental Procedures. For inhibition against NAD^+, NAD^+ concentrations ranging from 25 μM to 1.2 mM were used along with 1.2 mM AcH3 and varying concentrations of the inhibitor. For inhibition against AcH3, varying concentrations of inhibitor were mixed with AcH3 concentrations ranging from 25 μM to 1.2 mM and 1.2 mM NAD^+. The initial velocity data were fitted to three possible inhibition patterns based on the algorithms defined by Cleland (*32*): competitive (eq 4), noncompetitive (eq 5), and uncompetitive (eq 6).

$$v = (V_m[S])/\{K_m[1 + I/(K_{is} + [S])]\} \quad (4)$$

$$v = (V_m[S])/[K_m(1 + I/K_{is}) + [S](1 + I/K_{ii})] \quad (5)$$

$$v = (V_m[S])/[K_m + [S](1 + I/K_{ii})] \quad (6)$$

Rapid-Quench Analysis for Determining the Rates of Product Formation. The rates of *O*AADPr and nicotinamide formation were determined under single-turnover conditions using a Hi-Tech RQF-63 rapid-quench-flow device (Hi-Tech Scientific, Salisbusy, U.K.). Single-turnover reactions that included 325 μM NAD^+, 22.5 μM AcH3, 80 μM HST2, and 1 mM DTT were carried out at room temperature. Reactions were quenched with TFA to a final concentration of 1%. Radioactivity of fractions collected via reversed-phase HPLC was determined by scintillation counting. To determine the rate of *O*AADPR formation, [^{3}H]AcH3 was used as a substrate and the reactions were carried out between 60 and 1500 ms. The concentration of *O*AADPr was determined from the percentage of total radioactivity found in *O*AADPr and the initial [^{3}H]AcH3 concentration (22.5 μM). To determine the rate of nicotinamide formation, [^{14}C]NAD^+ was used as a substrate, and the formation of the [^{14}C]-nicotinamide was monitored between 10.3 and 8000 ms. The concentration of nicotinamide was determined by calculating the percentage of total radioactivity in the nicotinamide fraction and the initial [^{14}C]NAD^+ concentration (325 μM). To obtain the rate (k), the plot of product concentration formed over time was fitted to a single-exponential equation (eq 7), where P is the concentration of product formed, $[S]_0$ is the initial concentration of the limiting substrate, and t is the reaction time.

$$P = [S]_0(1 - e^{-kt}) \quad (7)$$

Synthesis of ^{14}C-Labeled NAD^+. [^{14}C]NAD^+, with the ^{14}C-carbonyl label on the nicotinamide moiety, was used for the rapid-quench analysis to determine the rate of nicotinamide formation. [^{14}C]NAD^+ was generated using the [^{14}C]nicotinamide$-NAD^+$ exchange reaction that was previously described (*8*, *27*, *29*). The reaction is performed at 37 °C in the presence of 20 μM HST2-H135A, 1 mM NAD^+, 100 μM AcH3, 200 μM [^{14}C]nicotinamide, and 1 mM DTT in 50 mM Tris at pH 7.5 and 37 °C. The reaction is quenched by the addition of TFA to a final concentration of 1%. The reaction mixture is then injected into the HPLC system with a reversed-phase column; substrates and products are eluted using the acetonitrile gradient described above, and radioactivity of the fractions collected is determined by scintillation counting. Fractions containing [^{14}C]NAD^+ are pooled, lyophilized, and resuspended in the desired buffer prior to use. The concentration of [^{14}C]NAD^+ is determined by measuring the absorbance at 260 nm, with NAD^+ having an ϵ_{260} of 18 mM^{-1} cm^{-1}.

Equilibrium Dialysis. Equilibrium dialysis was performed using Dispo-Equilibrium dialyzers from Harvard Bioscience. [^{3}H]AcH3 concentrations ranging from 10 to 300 μM were placed in the substrate chamber, while 25 μM HST2 was placed in the other chamber, with the total volume for each chamber being 75 μL. The dialyzers were rocked at 4 °C for at least 48 h. Control samples, where buffer was placed in the enzyme chamber, were also prepared to determine when equilibrium was reached, after which the radioactivities of samples from both chambers of the dialyzers were determined using scintillation counting. The concentrations of bound [^{3}H]AcH3 was plotted versus the concentrations of free [^{3}H]AcH3 and fitted into eq 8 using Kaleidagraph:

$$[\text{AcH3}\cdot\text{enzyme}] = ([\text{AcH3}\cdot\text{enzyme}]_{max}[\text{AcH3}])/(K_d + [\text{AcH3}]) \quad (8)$$

where [AcH3·enzyme] is the concentration of bound AcH3, $[\text{AcH3}\cdot\text{enzyme}]_{max}$ is the maximum concentration of bound AcH3, [AcH3] is the concentration of free AcH3, and K_d is the dissociation constant.

RESULTS

Catalytic Efficiency and Substrate Preference of Sir2 Enzymes. Substrate preferences and catalytic efficiencies of ySir2, HST2, and SIRT2 reactions were determined using a variety of monoacetylated histone H3 and H4 peptides (Table 1). H3 peptides acetylated at Lys-9 and -14 as well as H4 peptides acetylated at Lys-5, -8, -12, and -16 were employed, as these are known *in vivo* acetylation sites (*33*, *34*). The assays were performed under steady-state conditions (i.e., catalytic amounts of enzymes and rates calculated over the initial linear portion of product formation) in the presence of varying concentrations of the acetylated histone peptides and a saturating concentration of NAD^+. Deacetylation was assessed by either the charcoal binding assay or the HPLC-based assay. The plots of initial velocities versus peptide concentrations were fitted to the Michaelis−Menten equation

Table 1: Sequences of Peptide Substrates and Kinetic Parameters Obtained for the ySir2, HST2, and SIRT2 Reactions[a]

substrate	sequence	K_m (μM)			k_{cat} (s^{-1})[e]			k_{cat}/K_m (M^{-1} s^{-1})		
		ySir2	HST2	SIRT2	ySir2	HST2	SIRT2	ySir2	HST2	SIRT2
AcH3(K9)	ARTKQTAR(AcK)STGGKAPRKQL	239[d]	<2[b]	24 ± 4.2		0.32 ± 0.08	0.24 ± 0.03	(2.80[d] ± 0.48) × 10^3	> 1.6 × 10^5	(10.0 ± 2.2) × 10^3
AcH3(K14)	KSTGG(AcK)APRKQ	420 ± 40	4.3[c] ± 1.0	90[h] ± 15	0.67 ± 0.04			(1.6 ± 0.1) × 10^3	(56.7[g] ± 10.0) × 10^3	(13.0[h] ± 1.3) × 10^2
AcH3(K14)	ARTKQTARKSTGG(AcK)APRKQ		0.28 ± 0.01	54 ± 23.0					(71.8 ± 3.6) × 10^4	(39.3 ± 2.6) × 10^2
AcH4(K5)	SGRG(AcK)GGKGLGKGGAKRHRK	140 ± 32	<2[b]	48 ± 19				(4.2 ± 1.0) × 10^3	> 1.6 × 10^5	(36.0 ± 9.6) × 10^2
AcH4(K8)	SGRGKGG(AcK)GLGKGGAKRHRK	54 ± 17	<2[b]	24.9 ± 6.2				(12.8 ± 3.0) × 10^3	> 1.6 × 10^5	(7.2 ± 1.4) × 10^3
AcH4(K16)	SGRGKGGKGLGKGGA(AcK)RHRK	17.0 ± 5.0	<2[b]	25.5 ± 1.0				(43.8 ± 6.3) × 10^3	> 1.6 × 10^5	(9.4 ± 1.2) × 10^3
AcH4(K12)	SGRGKGGKGLG(AcK)GGAKRHRK	105 ± 15	<2[b]	141 ± 97	0.085 ± 004			810 ± 87	> 1.6 × 10^5	(29.0 ± 9.6) × 10^2
tubulin[f]	MPSD(AcK)TIGG				(2.5 ± 0.3) × 10^{-3}	0.144 ± 0.005		14.9 ± 5.4		(8.9 ± 1.0) × 10^2

[a] The k_{cat}/K_m values were obtained by fitting the data to the modified Michaelis−Menten equation, $v = [(k_{cat}/K_m)[S]]/(1 + [S]/K_m)$. [b] K_m values were too low for accurate determination using the HPLC-based assay. [c] The assay was performed using the charcoal binding assay; therefore, a K_m value was determined. This value is an average of K_m values obtained from saturation experiments as well as product inhibition analyses. [d] Only the k_{cat}/K_m value was obtained from the experiment. The K_m value was calculated from the k_{cat}/K_m value with the assumption that k_{cat} equaled 0.67 s^{-1}. [e] k_{cat} values are averages obtained from each of the peptide saturation curves. [f] k_{cat} and k_{cat}/K_m values were previously reported by North et al. (*19*). [g] The k_{cat}/K_m value is an average value obtained from saturation experiments as well as product inhibition analyses. [h] k_{cat}/K_m and K_m values are averages from multiple assays.

to determine the K_m, k_{cat}, and k_{cat}/K_m values (Table 1). The K_m is defined as the peptide concentration at half-maximal velocity; k_{cat} represents the overall first-order rate of the reaction at saturating levels of both NAD^+ and acetylated peptide, and k_{cat}/K_m is the second-order rate constant that represents the catalytic efficiency of the enzyme at low substrate concentrations. Average k_{cat} values of 0.67 ± 0.04, 0.32 ± 0.08, and 0.24 ± 0.03 s^{-1} were determined for ySir2, HST2, and SIRT2, respectively (Table 1), with the exception of ySir2 using AcH3(K9) and AcH4(K12). Because the k_{cat} values are similar, changes in the K_m reflect changes in the catalytic efficiency (k_{cat}/K_m). Because of the impractical requirement of high peptide concentrations for obtaining a saturation curve, only the k_{cat}/K_m value was obtained for ySir2 using AcH3(K9) as a substrate. A tubulin peptide was previously tested (*19*) as a substrate for SIRT2 and HST2, and the kinetic parameters are included in Table 1 for comparison.

Comparisons of k_{cat}/K_m values showed that the homologues exhibit varying catalytic efficiencies, with HST2 displaying the highest efficiency with all histone peptides that were examined. HST2, however, is approximately 6000-fold less efficient in utilizing the tubulin peptide than in utilizing histone peptides. For SIRT2, k_{cat}/K_m values range from 1300 to 10 000 M^{-1} s^{-1}, and ySir2 values range from 810 to 43 800 M^{-1} s^{-1}.

Within each enzyme data set, comparison of k_{cat}/K_m values for the different peptides shows that the enzymes display a substrate preference. For ySir2, there was a significant preference for the AcH4(K16) peptide, with a k_{cat}/K_m value 3−54-fold higher than those of the other histone peptides (Table 1). The next preferred substrate of ySir2 was the AcH4(K8) peptide, followed by AcH3(K9), AcH3(K14), and AcH4(K5), which were all similar. The worst substrate for ySir2 was AcH4(K12), as indicated by the enzyme's low efficiency. Although the K_m value for the AcH4(K12) peptide was within the range of values for the other peptides that were examined, the turnover rate (k_{cat}) was 1 order of magnitude lower (Table 1), suggesting that the residues surrounding the acetyllysine group may play a role in the rate-limiting step of the reaction. Although SIRT2 does not appear to display a preference between all of the histone peptides, it displayed less preference for the tubulin peptides. For HST2, the k_{cat}/K_m values for the AcH3(K9) peptide and all of the AcH4 peptides were not determined due to the high catalytic efficiency of the enzyme. The K_m values for these peptides were in the high nanomolar range, which are beyond the HPLC detection limit, and therefore, accurate k_{cat}/K_m values could not be obtained. However, using an upper estimate of 2 μM for the K_m value, we calculated a lower limit of 1.6 × 10^5 M^{-1} s^{-1} for the k_{cat}/K_m value for the AcH3(K9) and AcH4 peptides. Although the preference of HST2 for the AcH4 and AcH3(K9) peptides could not be determined, HST2 can discriminate between substrates, as shown by the significantly different efficiencies for the AcH3(K14) and tubulin peptides (Table 1).

Bisubstrate Kinetic Analysis. The members of the Sir2 family of NAD^+-dependent protein deacetylases catalyze a reaction involving two substrates, NAD^+ and acetylated protein, and three products, nicotinamide, deacetylated protein, and *O*AADPr (*9*, *10*). Despite the numerous mechanisms that have been suggested (*10*−*13*, *23*, *27*, *28*, *35*),

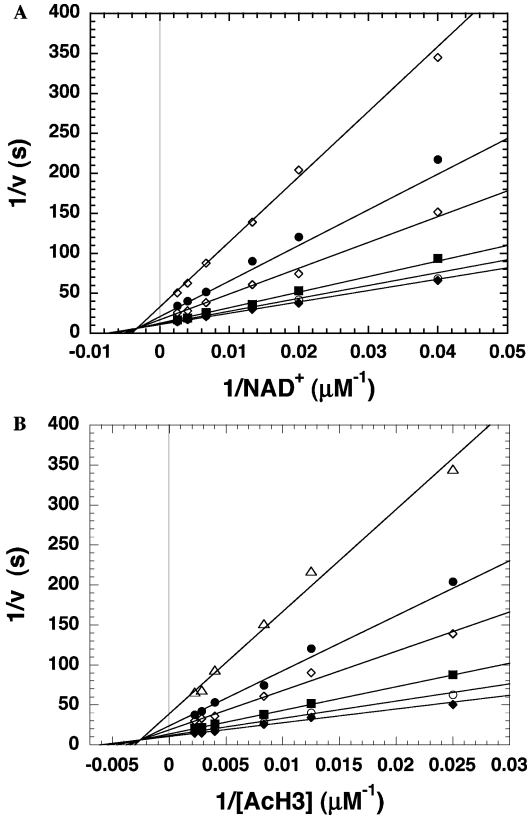

FIGURE 1: Formation of a ternary complex of SIRT2, NAD^+, and AcH3. The deacetylase assay was performed under steady-state conditions with varying NAD^+ and AcH3 concentrations. The data were fitted to the sequential mechanism using KinetAsyst software as described in Experimental Procedures. (A) Double-reciprocal plot of $1/v$ vs $1/[NAD^+]$ with the following AcH3 concentrations: (◇) 15, (●) 25, (◇) 50, (■) 75, (○) 125, and (◆) 200 μM. (B) Double-reciprocal plot of $1/v$ vs 1/[AcH3] with the following NAD^+ concentrations: (△) 25, (●) 50, (◇) 75, (■) 150, (○) 250, and (◆) 400 μM.

the kinetic mechanism for these enzymes has not been established. Bisubstrate kinetic analysis was performed to determine whether Sir2-like enzymes follow a sequential mechanism, where catalysis only proceeds after binding of both NAD^+ and acetylated substrate, or a ping-pong mechanism, where catalysis and product release occur, leaving a covalent enzyme intermediate, prior to the binding and reaction of the second substrate.

The bisubstrate kinetic analysis was performed under steady-state conditions, using SIRT2 with NAD^+ concentrations ranging from 25 to 400 μM and AcH3 (11-mer, monoacetylated at Lys-14) concentrations ranging from 40 to 450 μM. Initial velocities were measured, and double-reciprocal plots of $1/v$ versus 1/[substrate] were generated and fitted to a sequential or ping-pong kinetic mechanism. The plot of $1/v$ versus $1/[NAD^+]$ (Figure 1A) displays a series of lines that intersects to the left of the $1/v$ axis. A graph showing $1/v$ versus 1/[AcH3] shows a series of lines that intersects to the left of the $1/v$ axis, consistent with the sequential mechanism. A sequential mechanism was also determined from a bisubstrate kinetic analysis of HST2 (data not shown), suggesting a similar kinetic mechanism. The sequential mechanism requires that, prior to any catalytic step, both NAD^+ and the acetylated substrate bind to form a ternary complex with the enzyme.

Using the analysis described above, the K_m for NAD^+ was determined. We obtained the following K_m values for NAD^+: 82.6 ± 18.3 μM using SIRT2, 2.3 ± 0.6 μM using HST2, and 29.3 ± 8.6 μM for ySir2.

Inhibition Analyses. To establish the order of substrate binding and product release, product inhibition studies were performed. The concentrations of one substrate and of one product inhibitor were varied while the concentration of the other substrate was kept constant, and initial velocities were measured. The double-reciprocal plots of $1/v$ versus 1/[substrate] are fitted to competitive, uncompetitive, and noncompetitive equations to distinguish the mode of inhibition. The type of inhibition for the different substrate−product pairs can be diagnostic for determining the order of substrate binding and product release.

The products, nicotinamide and the deacetylated product, in this case, the unmodified H3 (11-mer) peptide, were used as inhibitors against NAD^+ and AcH3(K14). To determine the nicotinamide inhibition pattern versus NAD^+, initial velocities of the SIRT2-catalyzed reactions were measured at varying concentrations of nicotinamide and NAD^+, and at a constant concentration of AcH3. The plot of $1/v$ versus $1/[NAD^+]$ at various nicotinamide concentrations shows a series of lines intersecting to the left of the $1/v$ axis and above the $1/[NAD^+]$ axis, suggesting a noncompetitive inhibition (Figure 2A). The inhibition constants K_{ii} and K_{is} were 60 and 15 μM, respectively (Table 2). K_{is} and K_{ii} are noncompetitive inhibition constants, which reflect the effects of the inhibitor on the slope $[1/(k_{cat}/K_m)]$ and the intercept $(1/k_{cat})$ of a Lineweaver−Burke analysis, respectively. The different $1/v$ intercepts indicate that NAD^+ and nicotinamide can bind to different enzyme forms and that even high NAD^+ concentrations cannot overcome nicotinamide inhibition. The inhibition pattern of nicotinamide versus AcH3 was determined by varying nicotinamide and AcH3 concentrations in the presence of a constant NAD^+ concentration. The double-reciprocal plot of $1/v$ versus 1/[AcH3], which displayed a series of lines intersecting to the left of the $1/v$ axis and above the 1/[AcH3] axis, indicates noncompetitive inhibition (Figure 2B). The inhibition constants K_{ii} and K_{is} were 58 and 34 μM, respectively (Table 2). The inhibition pattern of the H3 peptide versus NAD^+ in a SIRT2-catalyzed reaction was determined by measuring the initial velocities at varied NAD^+ and H3 concentrations and at a constant AcH3 concentration. The graph of $1/v$ versus $1/[NAD^+]$ indicated that the H3 peptide is a noncompetitive inhibitor against NAD^+ (Figure 3A). To determine the inhibition pattern of the H3 peptide versus AcH3, the NAD^+ concentration was kept constant while the concentrations of H3 versus AcH3 were varied. The graph of $1/v$ versus 1/[AcH3] at varying H3 concentrations in an HST2-catalyzed reaction shows that the H3 peptide exhibits competitive inhibition toward AcH3 (Figure 3B). The inhibition of AcH3 by H3 in the SIRT2-catalyzed reaction also displayed a competitive inhibition pattern (data not shown). However, in both cases, we cannot rule out the possibility that there is a small intercept effect (noncompetitive component), which might be due to the formation of a nonproductive complex between NAD^+ and the H3 peptide. The recently determined crystal structure of Sir2-Af2 with bound p53 peptide and 2′-*O*AADPr (*23*) demonstrated that nonproductive complexes can form.

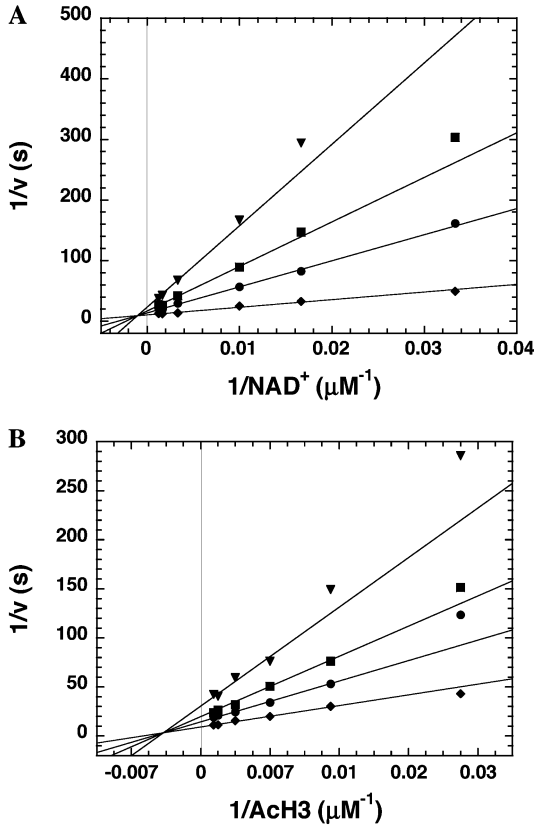

FIGURE 2: Nicotinamide exhibits noncompetitive inhibition toward NAD^+ (A) and AcH3 (B) during the SIRT2-catalyzed reaction. The charcoal binding assay was performed under steady-state conditions. (A) For nicotinamide inhibition toward NAD^+, the assay was performed in the presence of 1.2 mM AcH3, NAD^+ concentrations ranging from 30 to 800 μM, and the following nicotinamide concentrations: (▼) 100, (■) 50, (●) 25, and (◆) 0 μM. (B) For nicotinamide inhibition toward AcH3, the assay was performed in the presence of 1.2 mM NAD^+, AcH3 concentrations ranging from 40 to 800 μM, and the following nicotinamide concentrations: (▼) 100, (■) 50, (●) 25, and (◆) 0 μM. Data were fitted to noncompetitive inhibition using the KinetAsyst software as described in Experimental Procedures.

Table 2: Summary of Inhibition Constants[a]

inhibitor	substrate	type of inhibition	K_{ii} (μM)	K_{is} (μM)
nicotinamide	NAD^+	noncompetitive	60.5 ± 12.1	14.6 ± 2.2
nicotinamide	AcH3	noncompetitive	58.0 ± 3.1	34.3 ± 6.4
H3 peptide	NAD^+	noncompetitive	2500 ± 500	891 ± 162
H3 peptide	AcH3	competitive		194 ± 65
ADP-ribose	NAD^+	noncompetitive	1330 ± 180	657 ± 182
ADP-ribose	AcH3	noncompetitive	2620 ± 310	1280 ± 280
carba-NAD^+	NAD^+	noncompetitive	210 ± 20	170 ± 20

[a] For each inhibition analysis, the concentrations of the indicated substrate and the inhibitors were varied, while the concentration of the other substrate was kept constant. The initial velocities were plotted in a double-reciprocal plot of $1/v$ vs 1/[substrate] and fitted to the appropriate inhibitor equations using the KinetAsyst software.

*O*AADPr was also tested as a product inhibitor against NAD^+ (data not shown). *O*AADPr exhibited noncompetitive inhibition. However, the analysis is complicated by the fact that under these conditions there is an approximately 50:50 mixture of 2′- and 3′-*O*AADPr present in the reaction mixture. The enzymatic product of the reaction has been shown to be 2′-*O*AADPr (*11*−*13*, *23*), but in solution, 2′-OAADPr rapidly equilibrates, through a nonenzymatic transesterification reaction, with the 3′-*O*AADPr (*11*, *12*),

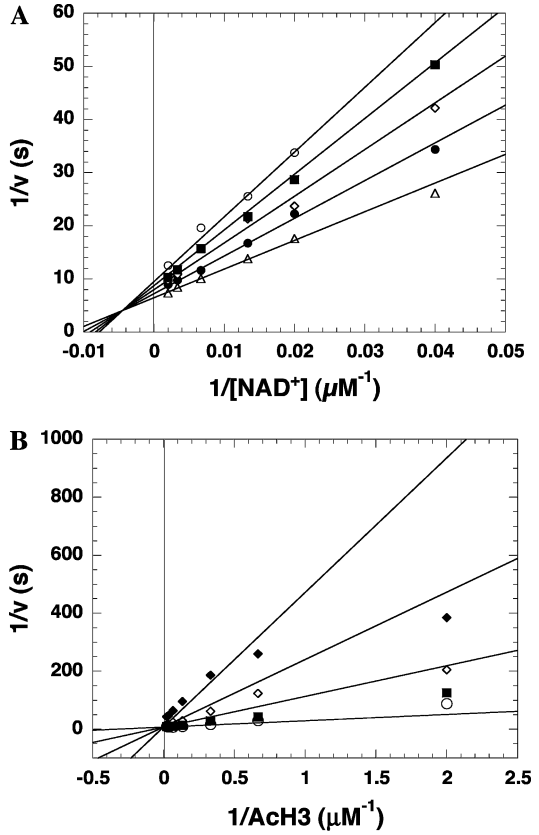

FIGURE 3: H3 vs NAD^+ and H3 vs AcH3. The charcoal binding assay was utilized to determine the H3 inhibition vs NAD^+ in a SIRT2-catalyzed reaction (A) and H3 inhibition vs AcH3 in a HST2-catalyzed reaction (B). (A) Reactions were performed using NAD^+ concentrations ranging from 25 to 500 μM and the following H3 peptide concentrations: (○) 1200, (■) 900, (◇) 600, (●) 300, and (△) 0 μM. (B) Reactions were performed using 200 μM NAD^+, AcH3 concentrations ranging from 0.5 to 45 μM, and the following H3 concentrations: (■) 9 mM, (O) 4.2 mM, (◆) 800 μM, and (◇) 0 μM.

which likely acts as a dead-end inhibitor, precluding accurate interpretation of the data.

The dead-end inhibitors ADP-ribose and carba-NAD^+, a nonhydrolyzable NAD^+ analogue, were also evaluated. ADPr was tested as an inhibitor against NAD^+ and AcH3 in a SIRT2-catalyzed reaction. ADPr displays noncompetitive inhibition versus NAD^+ (Figure 4A) and versus AcH3 (Figure 4B), with inhibition constants in the high micromolar and millimolar range (Table 2). To determine the inhibition pattern of carba-NAD^+ against NAD^+, the assay was performed using SIRT2 in the presence of varying carba-NAD^+ and NAD^+ concentrations and a constant AcH3 concentration. The double-reciprocal plot showed that carba-NAD^+ is a noncompetitive inhibitor against NAD^+ with K_{ii} and K_{is} values of 210 and 170 μM, respectively.

Equilibrium Dialysis in Assessing Substrate Binding. The binding of [^{14}C]NAD^+ and [^{3}H]AcH3 to the free enzyme was assessed using equilibrium dialysis. No NAD^+ binding was detected with HST2 at concentrations of up to 200 μM (data not shown). Similarly, using isothermal titration calorimentry (ITC), we detected no significant heats of binding with HST2 or SIRT2 when each was titrated with NAD^+ (up to 130 μM) (data not shown). Binding of [^{3}H]AcH3 to free HST2 was assessed using [^{3}H]AcH3 concentrations from 10 to 300 μM and 25 μM HST2. AcH3 bound independently

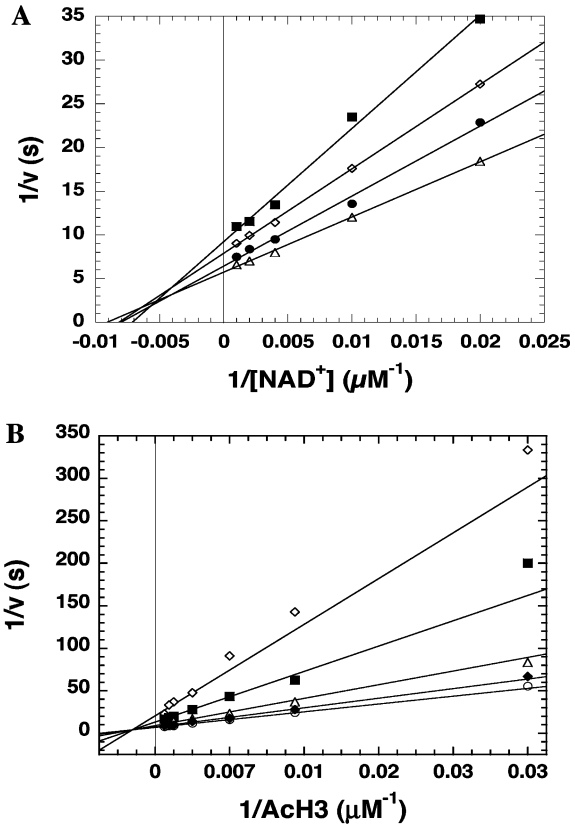

FIGURE 4: Dead-end inhibitor, ADPribose, exhibits noncompetitive inhibition of the SIRT2 reaction. The charcoal binding assay was utilized to assess the inhibiton of ADP-ribose toward NAD^+ and AcH3. (A) For ADP-ribose inhibition toward NAD^+, the assay was performed in the presence of 1.2 mM AcH3, NAD^+ concentrations ranging from 30 to 1000 μM, and the following ADP-ribose concentrations: (◇) 3000, (■) 1000, (△) 350, and (○) 0 μM. (B) For ADP-ribose inhibition toward AcH3, the assay was performed in the presence of 1.2 mM NAD^+, AcH3 concentrations ranging from 30 to 1200 μM, and the following ADP-ribose concentrations: (◇) 6500, (■) 3000, (△) 100, (◆) 300, and (○) 0 μM.

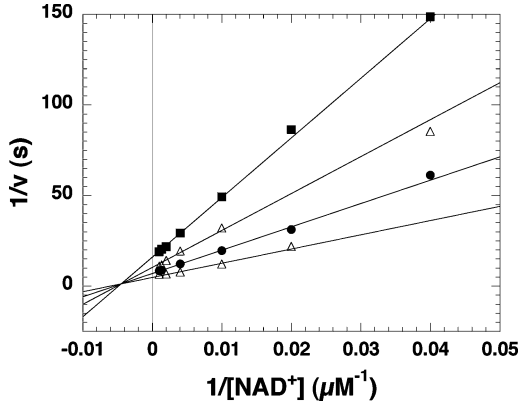

FIGURE 5: Nonhydrolyzable NAD^+ analogue, carba-NAD^+, exhibits a noncompetitive inhibition toward NAD^+ during a SIRT2-catalyzed reaction. The assay was performed in the presence of NAD^+ concentrations ranging from 25 to 1000 μM and the following carba-NAD^+ concentrations: (■) 500, (△) 250, (●) 100, and (△) 0 μM.

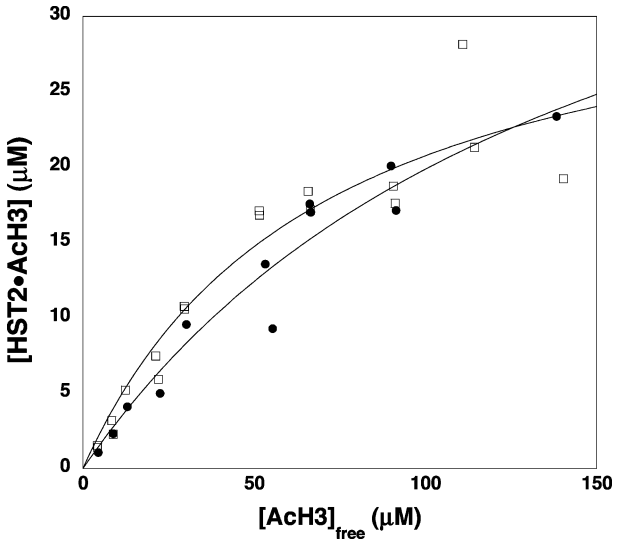

FIGURE 6: Binding of the acetylated substrate to the free enzyme. Varying concentrations of [^{3}H]AcH3, ranging from 10 to 300 μM, were placed in one chamber of the equilibrium dialyzers, while 25 μM HST2 was placed in the other (●). The dialyzers were rocked at 4 °C for at least 48 h. Radioactivity of each chamber was determined using scintillation counting, and the concentration of the bound [^{3}H]AcH3 was plotted vs the concentration of the free [^{3}H]AcH3. The same concentrations of [^{3}H]AcH3 and HST2 were placed in the dialyzers. ADP-ribose (1 mM) was added into each chamber to determine whether ADP-ribose binding has an effect on acetylated substrate binding (□).

to the free HST2 (Figure 6), with a K_d of 150 ± 63 μM. To determine whether ADP-ribose, as a mimic of NAD^+, would alter the enzyme's affinity for the acetylated peptide, a separate set of dialyzers were prepared in which 1 mM ADP-ribose was included in each of the chambers in addition to HST2 and [^{3}H]AcH3. Our results show that the presence of ADP-ribose did not have a significant effect on binding of AcH3 to the enzyme (Figure 6). The calculated K_d for AcH3 binding in the presence of ADP-ribose was 69 ± 20 μM, which was not significantly different than in the absence of ADP-ribose.

Rapid-Quench Analysis. A pre-steady-state, rapid-quenching kinetic analysis was preformed to provide mechanistic information about the individual steps involved in converting the ternary complex into products. The assays were performed under one limiting substrate concentration, thus allowing only a single turnover of the enzyme. The assays were performed in the presence of 80 μM HST2, 325 μM NAD^+, and 22.5 μM AcH3. Under these conditions, all the AcH3 is predicted to bind to the enzyme. At various times, reactions were quenched with TFA to a final concentration of 1%, and the products and reactants were resolved by HPLC. To determine the rate of nicotinamide formation, [^{14}C]NAD^+, with the ^{14}C label on the nicotinamide carbonyl group, was utilized, the reactions were carried out between 10.3 ms and 8 s, and the amounts of HPLC-resolved [^{14}C]-nicotinamide and [^{14}C]NAD^+ were quantified using scintillation counting. A plot of the concentration of nicotinamide formed versus time was fitted to a single-exponential equation to determine the rate of nicotinamide formation (Figure 7). Three separate experiments were performed with an average rate of 7.32 ± 0.72 s^{-1}. In all three experiments, the later time points do not fit well to a simple exponential equation, and an explanation for such a trend is discussed below. To determine the rate of *O*AADPr formation, the reaction was performed using [^{3}H]AcH3 from 60 ms to 15 s, and the amount of [^{3}H]*O*AADPr produced was determined using scintillation counting. A single-exponential fit of the *O*AADPr formed over time (Figure 7) yielded a rate of 1.26 ± 0.1 s^{-1} (average of two experiments).

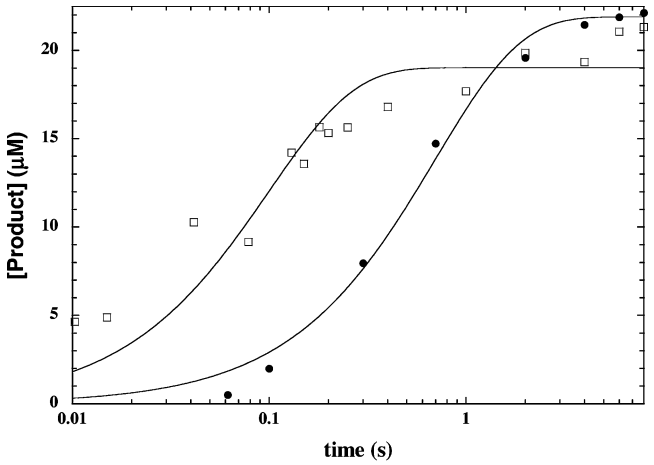

FIGURE 7: Rates of nicotinamide and *O*AADPR formation. Using a quench-flow apparatus, the HST2 reaction under single-turnover conditions was monitored on the millisecond time scale. Reactions were quenched with TFA, and substrates and products were resolved via reversed-phase HPLC. The reactions were carried out using 325 μM NAD^+, 22.5 μM AcH3, and 80 μM HST2 in 50 mM Tris (pH 7.5) with 1 mM DTT. To determine the rate of nicotinamide formation (□), [^{14}C]NAD^+ was used. Fractions from reversed-phase HPLC were subjected to scintillation counting to determine the amount of [^{14}C]nicotinamide formed and [^{14}C]NAD^+ left. A representative curve of nicotinamide formation from one of three experiments is shown. An average rate of 7.3 s^{-1} was determined from three separate experiments. To determine the rate of *O*AADPR formation (●), [^{3}H]AcH3 was used as a substrate. The amount of *O*AADPR formed and the amount of nicotinamide formed vs log time were fitted into a single-exponential equation to determine the rate of product formation.

DISCUSSION

Catalytic Efficiency and Substrate Preference of ySir2, HST2, and SIRT2. The recently determined crystal structures of an Archaea homologue, Sir2-Af2, bound to a p53 peptide (*22*), and of HST2 in a ternary complex with an acetylated histone H4 peptide and 2′-*O*AADPr (*23*) showed that the acetyllysine residue inserts into a hydrophobic tunnel, where the peptide backbones of the substrate and of the enzyme form hydrogen bonds, suggesting a minimal role for residues flanking the acetyllysine. The lack of specific interactions between the enzymes and the substrates in both crystal structures could be explained by the fact that p53 and histone are most likely not the physiological substrates for Sir2-Af2 and HST2, respectively. A more recently determined crystal structure of cobB bound to a histone H4 peptide suggests that the zinc-binding domain and regions outside the acetyllysine-binding site may contribute to substrate specificity (*35*).

Although some of our substrate specificity results support the crystallographic conclusions, most do not. The quantitative steady-state kinetic analysis, which allowed for investigation of the inherent differences in Sir2 enzymes with respect to monoacetylated histone H3 and H4 peptide substrates, revealed that Sir2 enzymes do indeed exhibit a substrate preference, albeit with varying catalytic efficiencies. Among the peptides that were examined, ySir2 displays the strongest preference for the AcH4(K16) peptide and the weakest preference for the AcH4(K12) peptide (Table 1). The human SIRT2 also exhibits a preference among the peptides that have been examined, with the strongest preference for AcH4(K12), AcH4(K16), and AcH4(K8) and the weakest preference for the tubulin peptide. Although the overall preference of HST2 for the histone peptides could not be determined because of its high catalytic efficiency, HST2 does display a substrate preference, as observed using the 11-mer and 20-mer AcH3(K14) peptide, respectively, compared to a 9-mer acetylated tubulin peptide.

The preference of ySir2 for Lys-5, -8, and -16 of the histone H4, with Lys-16 being the most preferred substrate, and the weakest preference for AcH4(K12) support previous cellular studies on silent chromatin domains. In *Saccharomyces cerevisiae*, immunoprecipitation of chromatin using antibodies specific for particular acetylated lysine residues of histone H4 revealed that lysines 5, 8, and 16 of histone H4 are hypoacetylated while lysine 12 shows significant acetylation (*36*). In addition, histone H3 was shown to be hypoacetylated (*36*). Previous biochemical data showing ySir2's preference for Lys-16 of histone H4 (*7*) also support our observation. Although our results indicate that the yeast homologue HST2 has higher catalytic efficiency for histone peptides than ySir2, it is important not to confuse catalytic efficiency with overall substrate preference or specificity. Likely, the accessory proteins in the complexes target ySir2 to the three silent loci, thereby increasing the effective substrate concentration and increasing the catalytic efficiency of the enzyme *in vivo*.

Recently, tubulin has been identified as an authentic substrate for SIRT2 (*19*). Although our results suggest that SIRT2 has slightly higher catalytic efficiency for some histone peptides than the tubulin peptide, SIRT2 appears to be specifically targeted to the microtubule network in the cytoplasm, which would result in an increased effective substrate concentration and an increased catalytic efficiency. In addition, although SIRT2 does not appear to discriminate between the 11-mer and 20-mer AcH3(K14) peptides, it is possible that the 9-mer tubulin peptide used in the previous study may be too short and thus results in an apparent decrease in the catalytic efficiency of SIRT2 *in vitro*.

Kinetic Mechanism of the Sir2 Reaction. Although several catalytic mechanisms have been proposed (*23*, *27*, *28*), the kinetic mechanism for this family of enzymes had not been investigated in detail. Here, we determined that Sir2-like enzymes (HST2 and SIRT2) follow a sequential mechanism, where the binding of both NAD^+ and acetylated substrate forms a ternary complex that is required prior to any chemical step. Essentially, this means that no covalent enzyme−substrate intermediate can form with either substrate alone. However, the sequential mechanism does not rule out the existence of enzyme−substrate intermediates once the ternary complex is formed.

Nicotinamide is the first product released by the enzyme, based on the ability of the Sir2 enzymes to catalyze a [^{14}C]-nicotinamide−NAD^+ exchange reaction (*8*, *27*−*29*) in the absence of the other two products. That is, nicotinamide can reverse the reaction in the absence of the deacetylated product and *O*AADPr in the reaction. The ability to catalyze [^{14}C]-nicotinamide−NAD^+ exchange is also consistent with the sequential mechanism, as no base exchange occurs in the absence of the acetylated substrate (*29*). Consistent with these results, our inhibition data show that nicotinamide exhibits noncompetitive inhibition with both NAD^+ and the acetylated substrate. We (*27*) and others (*37*) have also shown that nicotinamide is a noncompetitive inhibitor (versus NAD^+) with ySir2 and human SIRT1, suggesting that these enzymes

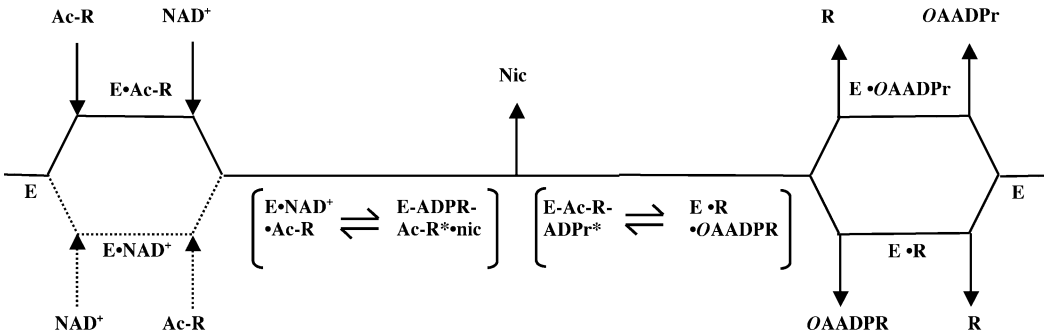

FIGURE 8: Proposed kinetic mechanism of the Sir2 reaction. Sir2 enzymes follow a sequential mechanism, in which both NAD^+ and the acetylated substrate (Ac-R) bind prior to any catalytic step. AcH3 is the preferred first substrate to bind, although NAD^+ could also bind to the free enzyme independently. Following formation of the ternary complex, nicotinamide is cleaved and released, leaving an enzyme−ADP-ribose-like intermediate, denoted by asterisks. The acetyl group from the acetylated substrate is then transferred to the ADP-ribose portion of NAD^+, forming *O*AADPr and the deacetylated product, which are released randomly.

employ the same basic kinetic mechanism. This fact is further supported by the identical H3 versus AcH3 inhibition pattern observed for both the HST2- and SIRT2-catalyzed reactions. The competitive inhibition displayed by H3 against AcH3 suggests that H3 is the last product released and AcH3 is the first to bind.

The noncompetitive inhibition displayed by ADP-ribose and carba-NAD^+ versus NAD^+ and the acetylated substrate indicates that these dead-end inhibitors can bind to an enzyme−deacetylated product complex. The existence of the enzyme−deacetylated product complex indicates that *O*AADPr is not the last product released in a fully ordered mechanism. The noncompetitive inhibition of the deacetylated product, histone H3 peptide, versus NAD^+ (Figure 3) suggests the existence of an enzyme−*O*AADPr complex, where binding of H3 to this complex in addition to binding to the free enzyme would result in the observed noncompetitive inhibition. Our inhibition analysis indicates that both the enzyme−*O*AADPr and enzyme−deacetylated product binary complexes can form during the reaction, suggesting that there is randomness in the release of the deacetylated product and *O*AADPr.

An equilibrium binding study showing that AcH3 can bind to the enzyme independently supports the idea that the acetylated substrate is the first to bind. Using equilibrium dialysis, we found that the acetylated peptide AcH3 can bind to the free enzyme with reasonable affinity ($K_d = 150\ \mu M$) (Figure 6). The inclusion of ADP-ribose in the dialysis did not affect the binding of AcH3 to the enzyme (Figure 6). Using both ITC and equilibrium dialysis, no significant binding of NAD^+ to HST2 or SIRT2 was detected up to 200 μM NAD^+. From these data, it appears that Sir enzymes demonstrate a preference for binding acetylated peptide first and NAD^+ second.

The crystal structure of HST2 in a nonproductive ternary complex with the acetylated histone and 2′-*O*AADPr (*23*) is consistent with our kinetic data, providing support for the formation of enzyme−acetylated substrate−ADP-ribose or carba-NAD^+ dead-end ternary complexes. Formation of these dead-end ternary complexes along with binding of ADP-ribose or carba-NAD^+ to the enzyme−deacetylated product complex would result in the noncompetitive inhibition observed in our analyses. After submission of this work, a paper showing the first ever structure of an intact NAD^+ molecule bound to a Sir2 enzyme was published (*38*). From this structural finding, it is postulated that NAD^+ binding is aided by the binding of the acetylated lysine substrate, a conclusion that is consistent with the data presented in this study.

From the available data, we propose the kinetic mechanism depicted in Figure 8. With SIRT2 and HST2 (and likely ySir2 and SIRT1), the acetylated substrate is the preferred first substrate to bind, followed by NAD^+. However, NAD^+ has been shown to bind archaeal Sir2 homologues in the absence of the second substrate, as indicated by various crystal structures (*13*, *24*, *38*). Whether this complex is productive has not been evaluated. Following the formation of the ternary complex and subsequent chemical catalysis, nicotinamide is released first followed by the random release of *O*AADPr and the deacetylated product.

Because of the absolute NAD^+ requirement for Sir2 activity, it has been postulated that the cellular NAD^+ levels affect Sir2 activity. We have obtained NAD^+ K_m values of 29, 90, and 2 μM for ySir2, SIRT2, and HST2, respectively. The K_m values for ySir2 and HST2 are similar to previously reported values (*39*), and are within the physiological range. In yeast, the NAD^+ concentration was estimated to be between 1.5 and 2 mM, although a significant percentage is in the bound form (*39*). In eukaryotes, NAD^+ is synthesized via two pathways: the de novo pathway using tryptophan and the salvage pathway in which degraded NAD^+ products are recycled (*3*, *40*). In yeast, it has been shown that steady-state NAD^+ levels do not change and that Sir2 activity may be modulated not by the de novo synthesis pathway but by the NAD^+ salvage pathway (*41*). Many of the NAD^+ salvage enzymes are located in the nucleus, and increased flux through this pathway is postulated to increase ySir2 activity.

Multistep Chemistry. Using rapid-quench analysis with HST2, we have provided the first direct kinetic evidence of multistep acetyl group transfer, with the kinetic resolution of an ADP-ribose-like intermediate. After formation of the ternary complex, nicotinamide is cleaved at a rate of 7.3 s^{-1} and subsequent formation of *O*AADPr occurs at 1.3 s^{-1}. The rate of nicotinamide formation does not fit perfectly to a single-exponential equation. The observed slowing of nicotinamide formation near the end of the reaction (Figure 7) is explained by the fact that cleavage of the nicotinamide ribosyl bond is a highly reversible step (*27*, *28*). As nicotinamide accumulates, it can condense with an enzyme−ADP-ribose-like intermediate to re-form NAD^+, resulting in the progressive slowing of nicotinamide formation. This explanation was verified using the kinetic simulation program

Specfit. From this simulation analysis, the rate of nicotinamide formation must be relatively fast, with a rate of ~10−20 s^{-1}. The rate at which nicotinamide condenses with the enzyme−ADP-ribose-like intermediate must be comparable to the forward rate. Previously, this was shown to be ~3 s^{-1} (*27*). Therefore, the trend in the data can be described by the efficient reversibility of this portion of the reaction.

The nature of an ADP-ribose-like intermediate was recently explored (*27*, *28*). Cleavage of the ribosyl−nicotinamide bond and release of free nicotinamide are thought to give rise to an imine adduct between the carbonyl oxygen of the acetylated substrate and C1 of the ribose ring. Alternatively, the intermediate could represent a stabilized oxocarbenium cation of ADP-ribose, which then would condense with the acetyl group to form the above-mentioned imine adduct. Subsequent attack of the ribose 2′-OH and addition of a water molecule would liberate the deacetylated substrate and 2′-*O*AADPr. The potent inhibition of the Sir2 reaction by nicotinamide (Table 2) and the efficient exchange reaction with NAD^+ support the idea of a distinct, ADP-ribose enzyme intermediate which can condense with exogenous nicotinamide to re-form NAD^+ and the acetylated substrate (*27*, *28*). The rate of this exchange reaction was estimated to be 2−3 s^{-1} at a saturating nicotinamide concentration (*27*, *28*). The apparent K_m for nicotinamide exchange was 38 μM with SIRT2 (*27*, *28*), a value that is similar to the inhibition constants (average of 42 μM) derived from the noncompetitive inhibition analyses listed in Table 2. Thus, this facile reaction between free nicotinamide and the ADP-ribose−enzyme intermediate results in robust inhibition of Sir2 enzymes, which has important physiological consequences. Nicotinamide was shown to be an *in vivo* inhibitor of Sir2 function, which caused accelerated aging in yeast (*37*). The product inhibitor nicotinamide promotes the partial reversal of the reaction to re-form NAD^+ and the acetylated substrate, inhibiting the forward reaction and the production of the deacetylated product and *O*AADPr.

Comparison of the rates of nicotinamide (7.3 s^{-1}) and *O*AADPr (1.3 s^{-1}) formation with the average turnover rate of approximately 0.2 s^{-1} indicates that the rate-limiting step in the reaction occurs after acetyl group transfer. Accordingly, the rate-limiting step may involve the physical release of *O*AADPr or the deacetylated product. The fact that most peptide substrates yield similar k_{cat} values suggests that a common step limits the overall turnover rate. This step could involve a slow conformational change that permits release of *O*AADPr, or this step could involve the last chemical transformation to generate 2′-*O*AADPr. Because the quench-flow analysis detected the formation of *O*AADPr upon rapid quenching of the enzyme, we cannot rule out the possibility that a labile intermediate, which collapsed to the observed *O*AADPr, was being formed in the reaction. Interestingly, residues flanking the acetyllysine substrate appear to affect the turnover rate of some enzymes with some substrates. For instance, ySir2 displays an approximately 8-fold lower k_{cat} value using AcH4(K12) compared to the average value (0.68 s^{-1}) using other histone H4 peptides (Table 1). Also, HST2 displays an ~126-fold lower k_{cat} value when a 9-mer α-tubulin peptide is used (*19*) than when the H3 and H4 peptides described in this study are used. Although it is not clear how residues adjacent to the acetyllysine could affect catalysis and/or product release, the surrounding side chains of these poor substrates may disrupt the optimal orientation of the acetyllysine side chain with respect to the bound NAD^+ and the catalytic residues on the enzyme such that catalysis or product release becomes rate-determining. Nevertheless, these data along with the differences in k_{cat}/K_m provide strong support for the inherent substrate discrimination harbored by the catalytic domains of Sir2 enzymes.

ACKNOWLEDGMENT

We thank Drs. Rolf Sterglanz, Eric Verdin, and Rui-Ming Xu for providing plasmids and Sir2 proteins. We are also grateful to Dr. C. D. Allis for providing the AcH3(K9) peptide and to Dr. Paul Cook for helpful discussions about the kinetic data.

REFERENCES

1. Kouzarides, T. (2000) Acetylation: a regulatory modification to rival phosphorylation? *EMBO J. 19*, 1176−1179.
2. Grozinger, C. M., and Schreiber, S. L. (2002) Deacetylase enzymes: biological functions and the use of small-molecule inhibitors, *Chem. Biol. 9*, 3−16.
3. Denu, J. M. (2003) Linking chromatin function with metabolic networks: Sir2 family of NAD^+-dependent deacetylases, *Trends Biochem. Sci. 28*, 41−48.
4. Moazed, D. (2001) Enzymatic activities of Sir2 and chromatin silencing, *Curr. Opin. Cell Biol. 13*, 232−238.
5. Frye, R. A. (1999) Characterization of five human cDNAs with homology to the yeast SIR2 gene: Sir2-like proteins (sirtuins) metabolize NAD and may have protein ADP-ribosyltransferase activity, *Biochem. Biophys. Res. Commun. 260*, 273−279.
6. Smith, J. S., Brachmann, C. B., Celic, I., Kenna, M. A., Muhammad, S., Starai, V. J., Avalos, J. L., Escalante-Semerena, J. C., Grubmeyer, C., Wolberger, C., and Boeke, J. D. (2000) A phylogenetically conserved NAD^+-dependent protein deacetylase activity in the Sir2 protein family, *Proc. Natl. Acad. Sci. U.S.A. 97*, 6658−6663.
7. Imai, S., Armstrong, C. M., Kaeberlein, M., and Guarente, L. (2000) Transcriptional silencing and longevity protein Sir2 is an NAD-dependent histone deacetylase, *Nature 403*, 795−800.
8. Landry, J., Sutton, A., Tafrov, S. T., Heller, R. C., Stebbins, J., Pillus, L., and Sternglanz, R. (2000) The silencing protein SIR2 and its homologs are NAD-dependent protein deacetylases, *Proc. Natl. Acad. Sci. U.S.A. 97*, 5807−5811.
9. Tanner, K. G., Landry, J., Sternglanz, R., and Denu, J. M. (2000) Silent information regulator 2 family of NAD-dependent histone/protein deacetylases generates a unique product, 1-O-acetyl-ADP-ribose, *Proc. Natl. Acad. Sci. U.S.A. 97*, 14178−14182.
10. Tanny, J. C., and Moazed, D. (2001) Coupling of histone deacetylation to NAD breakdown by the yeast silencing protein Sir2: Evidence for acetyl transfer from substrate to an NAD breakdown product, *Proc. Natl. Acad. Sci. U.S.A. 98*, 415−420.
11. Jackson, M. D., and Denu, J. M. (2002) Structural identification of 2′- and 3′-O-acetyl-ADP-ribose as novel metabolites derived from the Sir2 family of β-NAD^+-dependent histone/protein deacetylases, *J. Biol. Chem. 277*, 18535−18544.
12. Sauve, A. A., Celic, I., Avalos, J., Deng, H., Boeke, J. D., and Schramm, V. L. (2001) Chemistry of gene silencing: the mechanism of NAD^+-dependent deacetylation reactions, *Biochemistry 40*, 15456−15463.
13. Chang, J. H., Kim, H. C., Hwang, K. Y., Lee, J. W., Jackson, S. P., Bell, S. D., and Cho, Y. (2002) Structural basis for the NAD-dependent deacetylase mechanism of Sir2, *J. Biol. Chem. 277*, 34489−34498.
14. Luo, J., Nikolaev, A. Y., Imai, S., Chen, D., Su, F., Shiloh, A., Guarente, L., and Gu, W. (2001) Negative Control of p53 by Sir2α Promotes Cell Survival under Stress, *Cell 107*, 137−148.
15. Vaziri, H., Dessain, S. K., Eaton, E. N., Imai, S. I., Frye, R. A., Pandita, T. K., Guarente, L., and Weinberg, R. A. (2001) hSIR2-(SIRT1) Functions as an NAD-Dependent p53 Deacetylase, *Cell 107*, 149−159.
16. Langley, E., Pearson, M., Faretta, M., Bauer, U. M., Frye, R. A., Minucci, S., Pelicci, P. G., and Kouzarides, T. (2002) Human SIR2

deacetylates p53 and antagonizes PML/p53-induced cellular senescence, *EMBO J. 21*, 2383−2396.
17. Muth, V., Nadaud, S., Grummt, I., and Voit, R. (2001) Acetylation of TAF(I)68, a subunit of TIF-IB/SL1, activates RNA polymerase I transcription, *EMBO J. 20*, 1353−1362.
18. Starai, V. J., Celic, I., Cole, R. N., Boeke, J. D., and Escalante-Semerena, J. C. (2002) Sir2-dependent activation of acetyl-CoA synthetase by deacetylation of active lysine, *Science 298*, 2390−2392.
19. North, B. J., Marshall, B. L., Borra, M. T., Denu, J. M., and Verdin, E. (2003) The human Sir2 ortholog, SIRT2, is an NAD^+-dependent tubulin deacetylase, *Mol. Cell 11*, 437−444.
20. Braunstein, M., Rose, A. B., Holmes, S. G., Allis, C. D., and Broach, J. R. (1993) Transcriptional silencing in yeast is associated with reduced nucleosome acetylation, *Genes Dev. 7*, 592−604.
21. Gotta, M., Strahl-Bolsinger, S., Renauld, H., Laroche, T., Kennedy, B. K., Grunstein, M., and Gasser, S. M. (1997) Localization of Sir2p: the nucleolus as a compartment for silent information regulators, *EMBO J. 16*, 3243−3255.
22. Avalos, J. L., Celic, I., Muhammad, S., Cosgrove, M. S., Boeke, J. D., and Wolberger, C. (2002) Structure of a Sir2 enzyme bound to an acetylated p53 peptide, *Mol. Cell 10*, 523−535.
23. Zhao, K., Chai, X., and Marmorstein, R. (2003) Structure of the yeast Hst2 protein deacetylase in ternary complex with 2′-O-acetyl ADP ribose and histone peptide, *Structure 11*, 1403−1411.
24. Min, J., Landry, J., Sternglanz, R., and Xu, R. M. (2001) Crystal structure of a SIR2 homolog-NAD complex, *Cell 105*, 269−279.
25. Finnin, M. S., Donigian, J. R., and Pavletich, N. P. (2001) Structure of the histone deacetylase SIRT2, *Nat. Struct. Biol. 8*, 621−625.
26. Zhao, K., Chai, X., Clements, A., and Marmorstein, R. (2003) Structure and autoregulation of the yeast Hst2 homolog of Sir2, *Nat. Struct. Biol. 10*, 864−871.
27. Jackson, M. D., Schmidt, M. T., Oppenheimer, N. J., and Denu, J. M. (2003) Mechanism of nicotinamide inhibition and transglycosidation by Sir2 histone/protein deacetylases, *J. Biol. Chem.* (in press).
28. Sauve, A. A., and Schramm, V. L. (2003) Sir2 Regulation by Nicotinamide Results from Switching between Base Exchange and Deacetylation Chemistry, *Biochemistry 42*, 9249−9256.
29. Landry, J., Slama, J. T., and Sternglanz, R. (2000) Role of NAD^+ in the deacetylase activity of the SIR2-like proteins, *Biochem. Biophys. Res. Commun. 278*, 685−690.
30. Borra, M. T., O'Neill, F. J., Jackson, M. D., Marshall, B., Verdin, E., Foltz, K. R., and Denu, J. M. (2002) Conserved enzymatic production and biological effect of O-acetyl-ADP-ribose by silent information regulator 2-like NAD^+-dependent deacetylases, *J. Biol. Chem. 277*, 12632−12641.
31. Borra, M. T., and Denu, J. M. (2003) Quantitative assays for characterization of the Sir2 family of NAD^+-dependent Deacetylases, *Methods Enzymol. 376*, 171−187.
32. Cleland, W. W. (1977) Determining the chemical mechanisms of enzyme-catalyzed reactions by kinetic studies, *Adv. Enzymol. Relat. Areas Mol. Biol. 45*, 273−387.
33. Loidl, P. (1994) Histone acetylation: facts and questions, *Chromosoma 103*, 441−449.
34. Csordas, A. (1990) On the biological role of histone acetylation, *Biochem. J. 265*, 23−38.
35. Zhao, K., Chai, X., and Marmorstein, R. (2004) Structure and Substrate Binding Properties of cobB, a Sir2 Homolog Protein Deacetylase from *Escherichia coli*, *J. Mol. Biol. 337*, 731−741.
36. Braunstein, M., Sobel, R. E., Allis, C. D., Turner, B. M., and Broach, J. R. (1996) Efficient transcriptional silencing in *Saccharomyces cerevisiae* requires a heterochromatin histone acetylation pattern, *Mol. Cell. Biol. 16*, 4349−4356.
37. Bitterman, K. J., Anderson, R. M., Cohen, H. Y., Latorre-Esteves, M., and Sinclair, D. A. (2002) Inhibition of silencing and accelerated aging by nicotinamide, a putative negative regulator of yeast sir2 and human SIRT1, *J. Biol. Chem. 277*, 45099−45107.
38. Avalos, J. L., Boeke, J. D., and Wolberger, C. (2004) Structural basis for the mechanism and regulation of Sir2 enzymes, *Mol. Cell 13*, 639−648.
39. Bedalov, A., and Simon, J. A. (2003) Sir2 flexes its muscle, *Dev. Cell 5*, 188−189.
40. Lin, S. J., and Guarente, L. (2003) Nicotinamide adenine dinucleotide, a metabolic regulator of transcription, longevity and disease, *Curr. Opin. Cell Biol. 15*, 241−246.
41. Anderson, R. M., Bitterman, K. J., Wood, J. G., Medvedik, O., Cohen, H., Lin, S. S., Manchester, J. K., Gordon, J. I., and Sinclair, D. A. (2002) Manipulation of a nuclear NAD^+ salvage pathway delays aging without altering steady-state NAD^+ levels, *J. Biol. Chem. 277*, 18881−18890.

BI049592E